Int. J. Electrochem. Sci., 15 **(2020)** 16 – 25, doi: 10.20964/2020.01.13

International Journal of
ELECTROCHEMICAL
SCIENCE
www.electrochemsci.org

One-step synthesis of nitrogen, sulphur-codoped graphene as electrode material for supercapacitor with excellent cycling stability

Hangchun Deng, Meiwu Zhu, Tianxiang Jin, Chuanhong Cheng, Jugong Zheng[*]*, Yong Qian*[*]

Jiangxi Province Key Laboratory of Polymer Micro/Nano Manufacturing and Devices, East China University of Technology, Nanchang, Jiangxi, 330013, China.
[*]E-mail: yqianecit@163.com (Y. Qian), jgzheng@ecit.cn (J. Zheng)

Received: 5 August 2019 / *Accepted:* 11 October 2019 / *Published:* 30 November 2019

Doping of carbon-based materials with heteroatoms is an efficient method to increase their electrocatalytic activities. In the present study, a one-step solvothermal method to prepare nitrogen and sulfur co-doped graphene (NSG) using thiourea and graphene oxide (GO) as raw materials, has been reported. For supercapacitor applications, NSG exhibited higher capacitive properties compared to undoped graphene (UG). The as-fabricated material displayed superior gravimetric specific capacitance of 176.5 F/g at 1.0 A/g and also showed outstanding long-term cyclic stability (95.0% capacitive retention after 10000 cycles).

Keywords: nitrogen and sulfur co-doped graphene (NSG), supercapacitor, electrode material

1. INTRODUCTION

Nowadays, rapid consumption of fossil fuels has worsened the problem of air pollution. The development of green, environmentally friendly, and sustainable energy, as well as new energy-storage technologies is a big challenge [1-3]. Among various energy storage devices, supercapacitors have attracted significant attention because of their high energy density, ultra-fast charge and discharge rates, long-term cycle life, and excellent stability. These outstanding features have made them potentially useful for next-generation energy storage systems [4].

Generally electrochemical methods are sensitive, stable, and accurate [5, 6] and have been widely used in electrochemical sensors [7, 8], ultracapacitors [9, 10], and fuel cells [11-13]. Based on their mechanism of storage, supercapacitors are usually divided into electrochemical double-layer capacitors (EDLCs) and pseudocapacitors (PCs). EDLCs store energy by means of reversible ion adsorption, without undergoing any electrochemical reaction. On the other hand, PC is attributed to

faradaic charge transfer, due to fast surface redox reactions of capacitive materials. [14] It is generally believed that electrode materials are vital for the performance of capacitors. Electrode materials mainly include carbon materials [15], transition metal oxides [16, 17], and conducting polymers [18].

Carbonaceous materials, including activated carbon [12], carbon nanotubes [19], carbon aerogels [20], carbon spheres [21], and graphene [22], have outstanding electrical conductivity, high specific surface area (SSA), and satisfactory mechanical performance, due to which they are widely used in electrochemical field. Besides, doping of single or two heteroatoms (such as nitrogen, boron, iodine, sulfur, and phosphorus) into nanocarbons helps to improve the capacitive performance by forming active sites during the electrochemical process [23, 24]. Moreover, the charge density and electrode wettability can also be improved by doping heteroatoms into carbon lattices.

In this work, we report a convenient and efficient approach to fabricate graphene sheets co-doped with N and S having porous structures. By choosing S and N as dopants, this work provides co-doped graphene as an ideal electrode material with advantages such as: large number of electrochemical active-sites, superior electrical conductivity, and excellent chemical stability.

2. EXPERIMENTAL

2.1. Chemicals

Thiourea and ethylene glycol were obtained from Sigma-Aldrich. $KMnO_4$, KOH, $NaNO_3$, 98% H_2SO_4, 30% H_2O_2 and natural graphite powder were obtained from China Medicine Co. All reagents were of analytical grade.

2.2. Preparation of nitrogen and sulphur-codoped graphene (NSG)

Graphite powder was used as the starting material to prepare graphene oxide (GO) by modified Hummer's method [25, 26]. The NSG nanosheets were prepared by a facile solvothermal method. A mixture of GO powder (100 mg) and thiourea (1 g) was dispersed in 100 mL ethylene glycol and sonicated for 2 h. Next, the blend was transferred to a 200 mL dry autoclave and held at 150 °C overnight. Later, after cooling to 20~30 °C, the mixture was centrifuged, washed with deionized water 3~5 times, and then freeze-dried for 36 h. In the last step, the obtained intermediates were heated at 800 °C for 3h under argon atmosphere. For comparison, undoped graphene (UG) was prepared by the same procedure, however, in the absence of thiourea."

2.3. Electrochemical Properties

A three-electrode system was employed to analyze the electrochemical properties of samples. All the electrochemical tests were performed on a CHI 660E electrochemical workstation using 6.0 M KOH electrolyte solution. A saturated calomel electrode (SCE) and Pt wire served the reference and counter electrode, respectively. The working electrode was fabricated by mixing NSG (85 wt%) with

PTFE (5 wt%) and carbon black (CB, 10 wt%). It was then pressed onto the Ni foam (1 × 1.5 cm^2) and dried under vacuum. Cyclic voltammetry (CV) and galvanostatic charge/discharge (GCD) were carried out to evaluate the electrochemical performance of NSG electrode. Cs was calculated from the galvanostatic charge/discharge curves using eq. (1)

$$C = \frac{I \cdot t}{m \cdot \Delta U} \quad (1)$$

where, I represents the discharge current, t refers to discharge time, m represents the mass of the active material, and ΔU is the voltage window (here, ΔU = 0.8 V).

2.4. Materials characterization

TEM images were obtained using JEM-2100F transmission electron microscope. AFM images were recorded using tapping-mode AFM (Agilent 5500). SEM images were obtained by field emission scanning electron microscopy (FE-SEM, Hitachi S-4800) at 5~10 kV. The SSAs of the UG and NSG were determined by N_2 adsorption/desorption experiments using BET method. XPS analysis was carried out on a Thermo Fisher X-ray photoelectron spectrometer (Al Kα radiation source) and the analysis spot was 400 μm in diameter.

3. RESULTS AND DISCUSSION

3.1. Morphologies and Structure of NSG

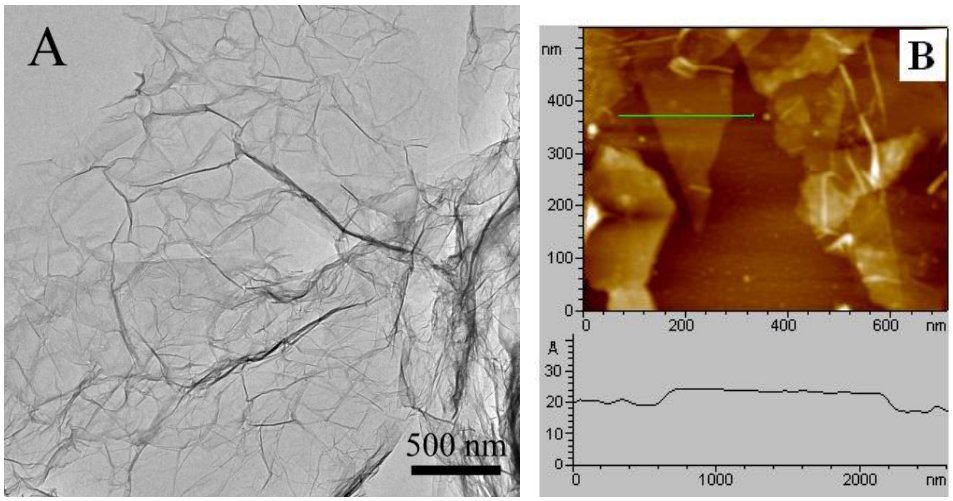

Figure 1. (A) TEM image of NSG, (B) AFM image and height profile of NSG

The morphological and structural analyses of NSG samples were conducted by TEM and AFM. The NSG sheets showed laminar creased silk-like features, which resembled the morphology of UG in our previous work. It was randomly stacked and compacted together as shown in Fig. 1A. This shape was due to defective structures or doped nitrogen and sulfur atoms in the NSG.

AFM can measure directly the shapes and the number of layers of NSG. The sample was prepared by dropping NSG in its aqueous suspension onto fresh mica and dried at 20~30 °C. Fig. 1B shows the AFM image of NSG. The average thickness of flattened NSG sheets was about 0.4 nm, corresponding to the thickness of a single-layered graphene (~0.34 nm).

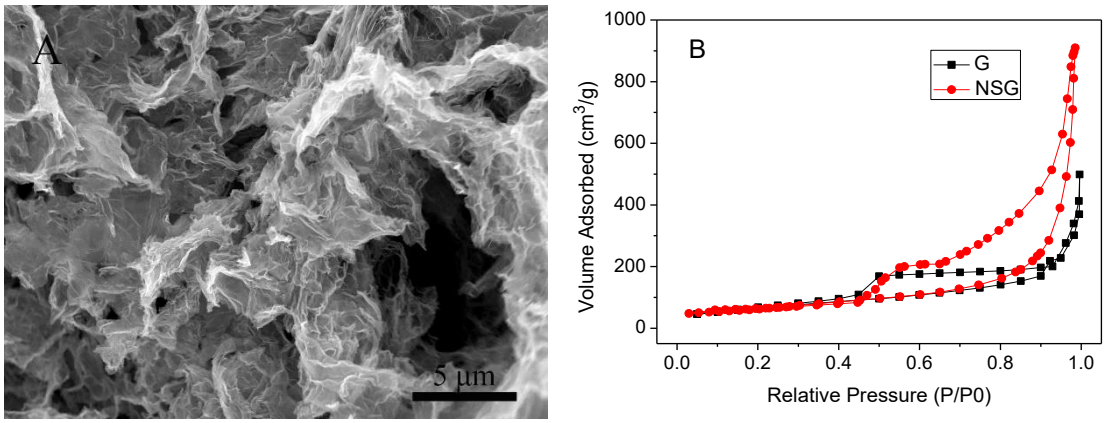

Figure 2. (A) SEM image of NSG, (B) N_2 adsorption-desorption plots of NSG and UG.

The NSG exhibited a fluffy, distinct, crumpled, and highly porous 3-D network structure with pore size ranging from submicron to several microns, as shown in Fig. 2A. The pore walls were very thin and were made up of many crumpled, randomly stacked graphene nanosheets. The surface of the carbon wall showed an interconnected porous structure with large number of mesopores and macropores, which were conducive for rapid diffusion of ions during the charge-discharge process.

The N_2 adsorption-desorption plots of NSG and UG samples showed type IV isotherms with high specific surface areas (SSAs) (Fig. 2B). The positive slope of the sample increased gradually in the range of relative pressure (P/P_0) from 0.4 to 0.8, which suggested that a large number of mesopores were present in NSG. A distinct increase in amount of adsorbed N_2 at $P/P_0 > 0.8$ could be attributed to the N_2 adsorbed in large-size pores. The SSA of NSG as determined by BET method was 392.5 m^2/g with total pore volume of 1.21 cm^3 /g, which was much higher than those for UG (263.5 m^2/g, 0.76 cm^3 /g).

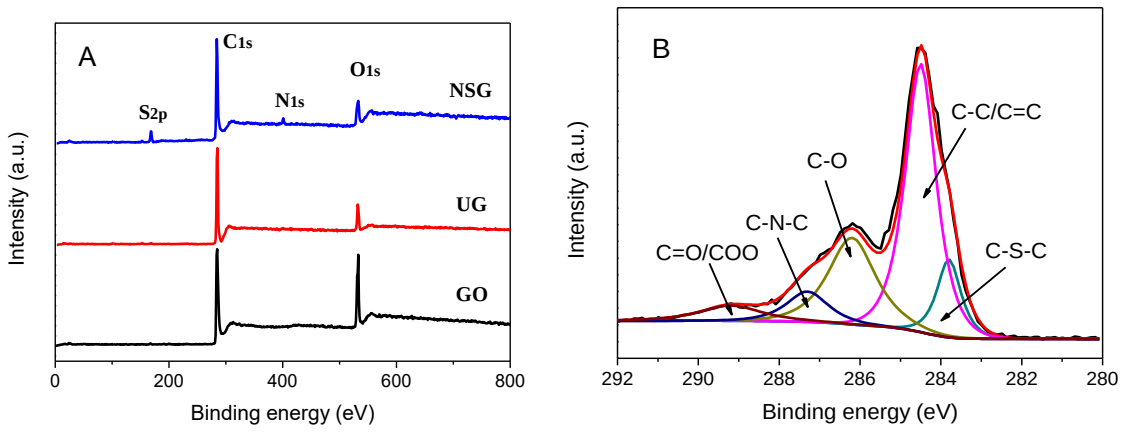

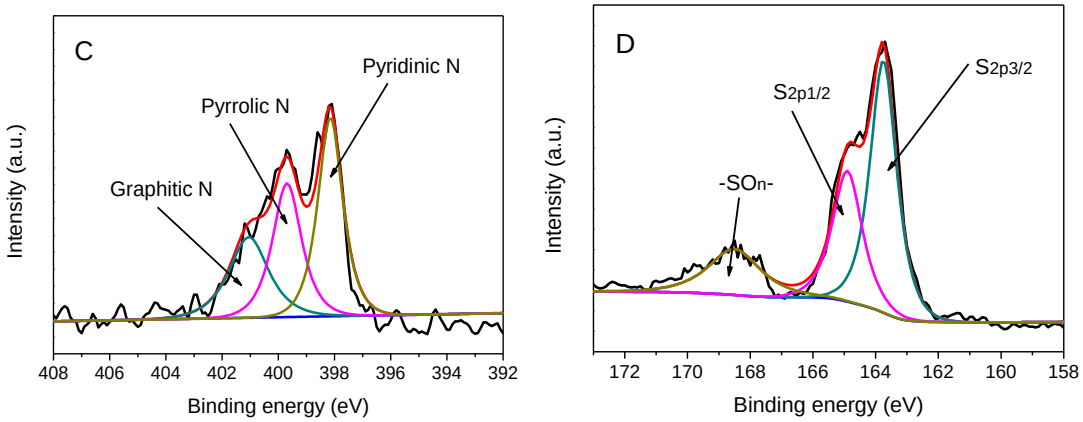

Figure 3. (A) XPS survey spectra of GO, UG, and NSG, (B) High-resolution XPS spectra of NSG (C) C 1s region, N 1s region, and (D) S 2p region.

The elemental composition and chemical states of NSG were investigated by XPS (Fig. 3A). The peaks at around 164, 285, 400, and 534.0 eV corresponded to sulfur, carbon, nitrogen, and oxygen elements, respectively. The wide-range XPS spectrum of NSG clearly showed two additional small peaks for S 2p and N 1s, when compared with GO and UG. This change indicated the successful chemical doping of nitrogen and sulfur atoms onto the frames of GO sheets. Furthermore, the O 1s peak for NSG and UG samples was much smaller than that for GO, indicating that the oxygen-containing functional groups of GO were partially eliminated or even disappeared in the hydrothermal process. The high resolution C 1s spectrum of NSG (Fig. 3B) could be deconvoluted into five peaks centered at 283.8, 284.5, 286.2, 287.3, and 289.2eV, corresponding to C−S−C, C−C/C=C (nonoxygenated carbon), C−O−C (epoxy), C−N−C, and C=O/COO, respectively. Peaks for C-S-C (283.8 eV) [27] and C-N-C (287.3 eV) [28] confirmed the doping of N and S heteroatoms into the carbon framework.

To further prove the nitrogen elemental composition, the high resolution N 1s spectrum of NSG was fitted with three different component peaks as shown in Fig. 3C, which corresponded to pyridinic-N (398.2 eV), pyrrolic-N (399.8 eV), and graphitic-N (401 eV). Sulfur atoms in NSG existed in two chemical states, as shown in Fig. 3D: thiophene-like S with neighboring carbon atoms and oxidized S (-SOn-). The two peaks centered at 163.8 eV and 164.9 eV were attributed to S 2p3/2 and S2p1/2 of thiophene-S, which is believed to play a key role in boosting the catalytic activity [29]. The peak positioned at 168.5 eV could be attributed to the presence of oxidized S [30]. According to literature, pyrrolic-N, pyridinic-N, and thiophenic-S help in boosting the pseudocapacitance through redox reactions, while graphitic-N improves the electroconductivity of carbon-based materials. [31]

3.2. Electrochemical Performance

The as-prepared NSG, due to its optimal SSA, hierarchical porous architecture, and moderate N, S dual doping, is expected to be an important carbonaceous material for supercapacitors. The cyclic

voltammetric (CV) curves of UG and NSG at 20 mV/s are presented in Fig. 4A. The shapes of CV were almost rectangular, which suggested that the material had excellent characteristics of double layer capacitance. Obviously, nitrogen, sulfur codoped graphene exhibited much greater curve area for current density than UG and hence the specific capacitance of NSG was more than that of UG. This could be due to codoping of nitrogen and sulfur, which increased the electrical conductivity and electrolyte solution wettability of graphene, and thus boosted the capacitance significantly.

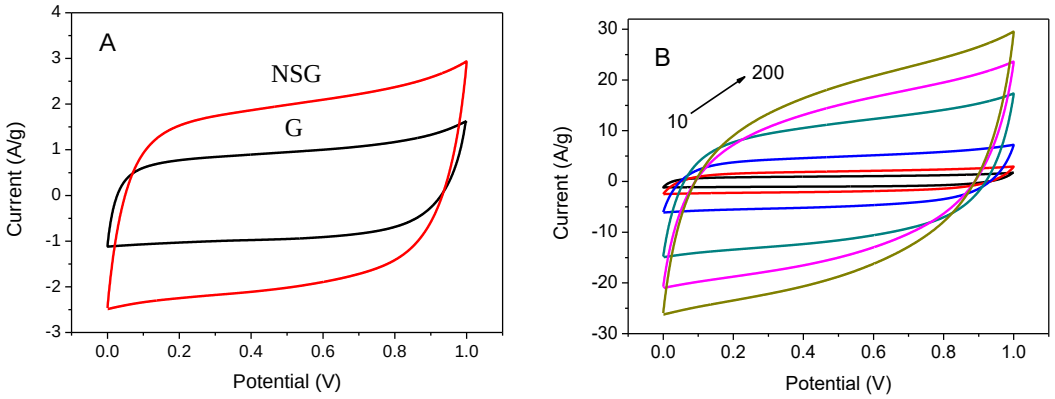

Figure 4. (A) CV curves of UG and NSG, measured at 20 mV/s in 6 mol/L aqueous KOH solution. (B) CV profiles of NSG measured at the different scan rates 10~200 mV/s. The arrows indicate the direction of increasing scan rates.

Therefore, it is important to study the supercapacitor properties of nitrogen and sulfur codoped graphene. Fig. 4B presents the CV profiles of NSG in the potential range of 0.0−1.0 V at sweep speed of 10−200 mV/s. The current response increased corresponding to increase in sweep speed. Moreover, the CV profiles remained quasi-rectangular even at 200 mV/s, without any drastic changes, indicating the good performance. This could be ascribed to the hierarchical porous structures that favored rapid diffusion of electrolyte ions through the entire NSG electrode.

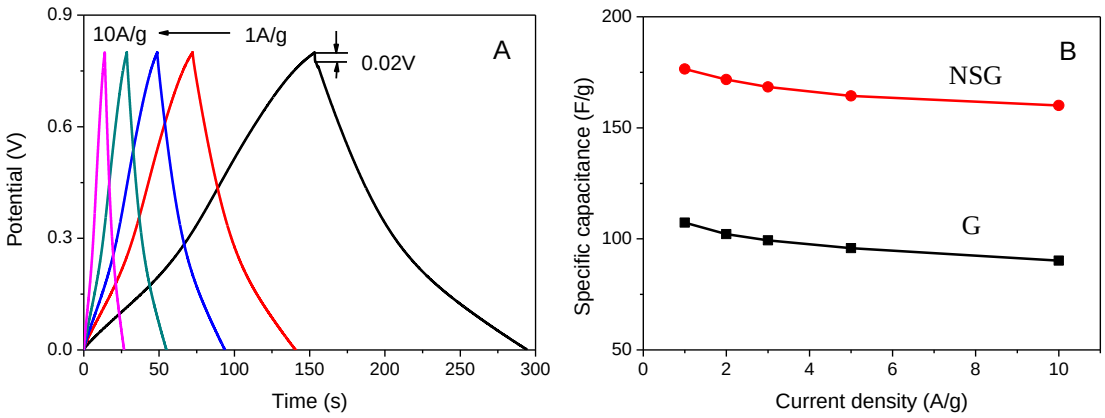

Figure 5. (A) GCD curves of the as-obtained NSG at various current densities from 1 to 10 A/g, (B) specific capacitances calculated from GCD curves.

Table 1. Partial list of reported carbon-based materials for Cs values

Carbon-based materials	Electrolyte	C_s (F/g)	Reference
N-doped carbon nanosheets	0.5M H_2SO_4	102 (25 mV/s)	[33]
Chemically-reduced graphene	6 M KOH	106.3(25mV/s)	[34]
nitrogen-doped graphene	6 M KOH	102(2 A/g)	[35]
lignin-derived HPC	1 M H_2SO_4	165 (0.05A/g)	[36]
lignin-derived HPC	1 M H_2SO_4	123.5 (10A/g)	[36]
Boron-doped carbon using SBA-15	6 M KOH	127 (2 mV/s)	[37]
HPC derived glucose	1 M H_2SO_4	140 (200mV/s)	[38]
MC derived from gelatin	6 M KOH	135 (20A/g)	[39]
NSG	6 M KOH	176.5 (1 A/g)	this study

HPC: hierarchical porous carbon, MC: mesoporous carbon

The capacitance of NSG was tested and evaluated by GCD method. Fig. 5A shows the curves for NSG from 0 to 0.8 V at various current densities. All GCD curves were symmetrically triangular in shape, which is electrochemical characteristic of an ideal EDLC. A very small voltage drop of about 0.02 V was observed clearly at the start of discharge at 1.0 A/g, suggesting a low internal resistance of NSG electrodes. The Cs obtained from galvanostatic discharge profiles are shown in Fig. 5B. As expected, the current density increased with decrease in Cs value, due to the decrease in ion accessible electroactive surface. [32]

The Cs value for NSG was 176.5 F/g at 1 A/g, which was significantly higher than that of UG (107.3 F/g). The NSG also showed outstanding rate capability (160.3 F/g remained at 10 A/g. In addition, the as-prepared NSG was compared with other similar carbons, reported in literature and the results are presented in Table 1. Evidently, the NSG electrode in this work exhibited a higher Cs than other carbon-based materials.

The NSG electrode material displayed good electrochemical properties, which could be attributed to its hierarchical porous structure with moderate SSA and a large number of interconnecting nitrogen and sulfur atoms. Firstly, porous structures with medium SSA could provide a larger number of accessible active sites to store a larger amount of charge, which contributed to higher Cs. Secondly, the large volume of macropores could be used as ion buffer reservoirs, which greatly reduced the distance for transport of ions to the inner surface. Finally, a large number of extensive N and S functional groups assisted not only to increase the surface hydrophilicity of carbon materials, but also provided a certain amount of pseudocapacitance, and helped in improving the capacitance performance.

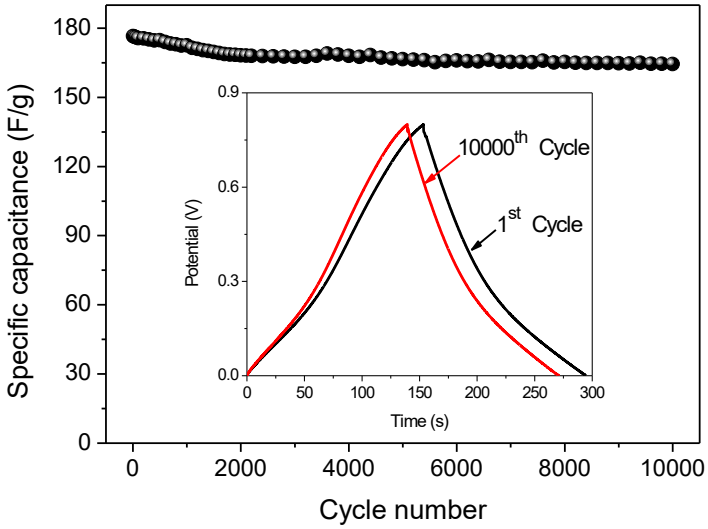

Figure 6. Cyclic stability of NSG electrode in 6 M KOH electrolyte solution at 1 A/g.

Life-cycle of an electrode is an important parameter in the daily applications of electrode materials for energy storage devices. The cyclic stability test was carried out by generating 10000 continuous GCD cycles for NSG in KOH electrolyte solution at 1 A/g. The curves recorded before and after successive 10000 cycles were compared, as shown in Fig. 6. The Cs of NSG remained 164.42 F/g, with retention of 93.1% after 10000 charge/discharge cycles, indicating outstanding cyclic stability. The decrease in Cs could be due to the swelling and shrinkage during the continuous charge/discharge process.

4. CONCLUSIONS

Nitrogen and sulfur co-doped graphene (NSG) was prepared by an effective solvothermal method and used as an electrode material for high-performance supercapacitor. The process was convenient, cost-effective, and did not use any catalyst or reducing agent. The NSG capacitive feature could be effectively regulated morphologically, structurally, and nitrogen and sulfur contents. NSG showed better capacitance performance than that of UG, wherein the gravimetric Cs of 176.5 F/g could be achieved at 1.0 A/g, along with excellent long-term cyclic stability (95.0% capacitive retention after 10000 cycles) of capacitive performance. The excellent capacitive characteristics coupled with its simple and economic preparation technique demonstrated the greater potential of NSG in the field of energy storage.

ACKNOWLEDGEMENTS
This work was jointly supported by NSFC (41562021), NSF of Jiangxi Province (20171BAB206016, 20161BAB204191), and The Foundation of Jiangxi Educational Committee (GJJ160565).

References

1. K. Xie, B. Wei, *Adv. Mater*, 26 (2014) 3592.
2. D. Yu, K. Goh, H. Wang, L. Wei, W. Jiang, Q. Zhang, L. Dai, Y. Chen, *Nat. Nanotechnol*, 9 (2014) 555.
3. X. B. Cheng, J. Q. Huang, Q. Zhang, H. J. Peng, M. Q. Zhao, F. Wei, *Nano Energy*, 4 (2014) 65.
4. Q. Wang, J. Yan, Z. J. Fan, *Energy Environ. Sci.*, 9 (2016) 729.
5. Y. Qian, C. Wang, F. Gao, *Biosens. Bioelectron*, 63 (2015) 425.
6. Y. Qian, D. Tang, L. Du, Y. Zhang, L. Zhang, F. Gao, *Biosens. Bioelectron*, 64 (2015) 177.
7. L. Ge, W. X. Wang, F. Li, *Anal. Chem.*, 89 (2017) 11560.
8. J. F. Chang, X. Wang, J. Wang, H. Y. Li, F. Li, *Anal. Chem.*, 91 (2019) 3604.
9. J. F. Chen, T. Zhu, X. P. Fu, G. Y. Ren, C. Y. Wang, *Int. J. Electrochem. Sci.*, 14 (2019) 7293.
10. Y. Qian, C. L. Huang, R. Chen, S. Z. Dai, C. Y. Wang, *Int. J. Electrochem. Sci.*, 11 (2016) 7453.
11. S. F. Zhao, P. P. Gai, W. Yu, H. Y. Li, F. Li, *Chem. Commun.*, 55 (2019) 1887.
12. M. W. Zhu, Q. Shao, Y. C. Pi, J. Guo, B. Huang, Y. Qian, X. Q. Huang, *Small*, 13 (2017) 1701295.
13. T. Zhu, J. B. Ding, Q. Shao, Y. Qian, X. Q. Huang, *ChemCatChem*, 11 (2019) 689.
14. V. H. Pham, J. H. Dickerson, *J. Phys. Chem. C*, 120 (2016) 5353.
15. L. Zheng, K. S. Xia, B. Han, C. G. Zhou, Q. Gao, H. Q. Wang, S. Pu, J. P. Wu, *ACS Appl. Nano Mater.*, 1 (2018) 6742−6751.
16. B. Huang, C. L. Huang, Y. Qian, *Int. J. Electrochem. Sci.*, 12 (2017) 11171.
17. Z. Huang, Y. Song, D. Feng, Z. Sun, X. Sun, X. Liu, *ACS Nano*, 12 (2018) 3557.
18. L. L. Wen, K. Li, J. J. Liu, Y. S. Huang, F. X. Bu, B. Zhao, Y. X. Xu, *RSC Adv.*, 7 (2017) 7688.
19. J. P. Xu, D. J. Huang, L. F. Nie, C. Y. Wang, Z. H. Xu, *Int. J. Electrochem. Sci.*, 11 (2016) 944.
20. G. Y. Ren, Q. S. Chen, J. G. Zheng, B. Huang, Y, Qian, *J. Electroanal. Chem.*, 829 (2018) 177.
21. G. Y. Ren, Y. N. Li, Q. S. Chen, Y. Qian, J. G. Zheng, Y. Zhu, C. Teng, *ACS Sustainable Chem. Eng.*, 6 (2018) 16032.
22. Y. Xie, Y. H. Yu, L. M. Lu, X. Ma, L. Gong, X. G. Huang, G. b. Liu, Y. F. Yu, *J. Electroanal. Chem.*, 812 (2018) 82.
23. L. M. Dai, Y. H. Xue, L. T. Qu, H. J. Choi, J. B. Baek, *Chemical Reviews*, 115 (2015) 4823.
24. X. D. Yan, Y. H. Yu, S. K. Ryu, J. L. Lan, X. L. Jia, X. P. Yang, *Electrochimica Acta*, 136 (2014) 466.
25. W. S. Hummers, R. E. Offeman, *J. Am. Chem. Soc.*, 80 (1958) 1339.
26. Y. Qian, F. Ye, J. Xu, *Int. J. Electrochem. Sci.*, 7 (2012) 10063.
27. S. Wan, L. Wang, Q. Xue, *Electrochem.Commun.* 12 (2010) 61.
28. Y. Zheng, Y. Jiao, J. Chen, J. Liu, J. Liang, A. Du, W. Zhang, Z. Zhu, S. C. Smith, M. Jaroniec, G. Q. Lu, S. Z. Qiao, *J. Am. Chem. Soc.* 133 (2011) 20116.
29. F. Buckel, F. Effenberger, C. Yan, A. Golzhauser, M. Grunze, *Adv Mater.*, 12 (2000) 901.
30. C. H. Choi, S. H. Park, S. I. Woo, *Green Chem*., 13 (2011) 406.
31. L. Sun, C. Tian, Y. Fu, J. Yin, L. Wang, H. Fu, *Chem. Eur. J*., 20 (2014) 564.
32. U. B. Nasini, V. G. Bairi, S. K. Ramasahayam, S. E. Bourdo, T. Viswanathan, A. U. Shaikh, *J. Power Sources*, 250 (2014) 257.
33. Y. Lee, Y. Lee, K. Chang, C. Hu, *Electrochem. Commun*., 13 (2011) 50.
34. Z. Wen, X. Wang, S. Mao, Z. Bo, H. Kim, S. Cui, G. Lu, X. Feng, J. *Chen, Adv. Mater.*, 24 (2012) 5610.
35. B. J. Jiang, C. G. Tian, L. Wang, L. Sun, C. Chen, X. Z, Nong, Y. J. Qiao, H. G. Fu, *Appl. Surf. Sci.*, 258 (2012) 3438.
36. W. Zhang, H. Lin, Z. Lin, J. Yin, H. Lu, D. Liu, M. Zhao, *ChemSusChem*, 8 (2015) 2114.
37. D. Wang, F. Li, Z. Chen, G. Lu, H. Cheng, *Chem. Mater.*, 20 (2008) 7195.
38. L. Estevez, R. Dua, N. Bhandari, A. Ramanujapuram, P. Wang, E. P. Giannelis, *Energ. Environ.*

Sci., 6 (2013) 1785.
39. B. Xu, S. Hou, F. Zhang, G. Cao, M. Chu, Y. Yang, *J. Electroanaly. Chem.*, 712 (2014) 146.